



MV/cm terahertz pulses from relativistic laser-plasma interaction characterized by nonlinear terahertz absorption bleaching in *n*-doped InGaAs

SUDIPTA MONDAL,^{1,2} HASSAN A. HAFEZ,^{1,3,4} XAVIER ROPAGNOL,¹ AND TSUNEYUKI OZAKI^{1,*}

¹Institut National de la Recherche Scientifique – Centre Energie, Matériaux et Télécommunications, 1650 Boulevard Lionel-Boulet, Varennes, Québec J3X 1S2, Canada

²ELI-ALPS, ELI-Hu Kft., Dugonics ter 13, H-6720 Szeged Hungary

³Max Planck Institute for Polymer Research, Ackermannweg 10, 55128 Mainz, Germany

⁴Physics Department, Faculty of Science, Helwan University, 11792, Cairo, Egypt

*ozaki@emt.inrs.ca

Abstract: We have developed a tabletop intense broadband terahertz (THz) source in the medium frequency range (≤ 20 THz) based on the interaction of a high-intensity femtosecond laser with solid targets at relativistic laser intensities. When an unpolished copper target is irradiated with a high-intensity femtosecond laser, a maximum of ~ 2.2 μJ of THz pulse energy is collected and detected with a calibrated pyroelectric detector. The THz spectrum was measured by using a series of bandpass filters, showing a bandwidth of ~ 7.8 THz full-width at half-maximum (FWHM) with a peak at ~ 6 THz. With tight focusing to reach high field strengths, we have demonstrated THz nonlinearity exemplified by THz absorption bleaching in a heavily *n*-doped InGaAs thin film, which enabled us to estimate the peak electric field of the THz pulses. We simulated the experimentally observed bleaching by employing a THz pulse having a bandwidth similar to that measured in our experiments and a temporal profile recoded in single-shot electro-optic detection. Through the simulations, we estimate a peak electric field associated with the THz pulses to be 2.5 MV/cm.

©2017 Optical Society of America

OCIS codes: (350.5400) Plasmas; (350.5610) Radiation; (260.3090) Infrared, far; (320.7090) Ultrafast lasers.

References and links

1. W. L. Kruer, *The Physics of Laser Plasma Interactions* (Addison-Wesley, 1988), Vol. 70.
2. P. Gibbon, *Short Pulse Laser Interactions with Matter* (Imperial College Press, 2005).
3. J. C. Kieffer and M. Chaker, "X-ray sources based on subpicosecond-laser-produced plasmas," *J. XRay Sci. Technol.* **4**(4), 312–322 (1994).
4. S. Corde, K. Ta Phuoc, G. Lambert, R. Fitour, V. Malka, A. Rousse, A. Beck, and E. Lefebvre, "Femtosecond x rays from laser-plasma accelerators," *Rev. Mod. Phys.* **85**(1), 1–48 (2013).
5. V. Malka, J. Faure, Y. A. Gauduel, E. Lefebvre, A. Rousse, and K. T. Phuoc, "Principles and applications of compact laser-plasma accelerators," *Nat. Phys.* **4**(6), 447–453 (2008).
6. E. Esarey, C. B. Schroeder, and W. P. Leemans, "Physics of laser-driven plasma-based electron accelerators," *Rev. Mod. Phys.* **81**(3), 1229–1285 (2009).
7. L. Robson, P. T. Simpson, R. J. Clarke, K. W. D. Ledingham, F. Lindau, O. Lundh, T. McCanny, P. Mora, D. Neely, C.-G. Wahlström, M. Zepf, and P. McKenna, "Scaling of proton acceleration driven by petawatt-laser-plasma interactions," *Nat. Phys.* **3**(1), 58–62 (2007).
8. A. Macchi, M. Borghesi, and M. Passoni, "Ion acceleration by superintense laser-plasma interaction," *Rev. Mod. Phys.* **85**(2), 751–793 (2013).
9. J. Faure, Y. Glinec, A. Pukhov, S. Kiselev, S. Gordienko, E. Lefebvre, J. P. Rousseau, F. Burgy, and V. Malka, "A laser-plasma accelerator producing monoenergetic electron beams," *Nature* **431**(7008), 541–544 (2004).
10. H. Hamster, A. Sullivan, S. Gordon, W. White, and R. W. Falcone, "Subpicosecond, electromagnetic pulses from intense laser-plasma interaction," *Phys. Rev. Lett.* **71**(17), 2725–2728 (1993).
11. Z. M. Sheng, K. Mima, and J. Zhang, "Powerful terahertz emission from laser wake fields excited in inhomogeneous plasmas," *Phys. Plasmas* **12**(12), 123103 (2005).
12. X. Xie, J. Xu, J. Dai, and X. C. Zhang, "Enhancement of terahertz wave generation from laser induced plasma," *Appl. Phys. Lett.* **90**(14), 141104 (2007).

13. K. Y. Kim, J. H. Glowina, A. J. Taylor, and G. Rodriguez, "Terahertz emission from ultrafast ionizing air in symmetry-broken laser fields," *Opt. Express* **15**(8), 4577–4584 (2007).
14. A. Gopal, P. Singh, S. Herzer, A. Reinhard, A. Schmidt, U. Dillner, T. May, H. G. Meyer, W. Ziegler, and G. G. Paulus, "Characterization of 700 μ J T rays generated during high-power laser solid interaction," *Opt. Lett.* **38**(22), 4705–4707 (2013).
15. G. Q. Liao, Y. T. Li, C. Li, L. N. Su, Y. Zheng, M. Liu, W. M. Wang, Z. D. Hu, W. C. Yan, J. Dunn, J. Nilsen, J. Hunter, Y. Liu, X. Wang, L. M. Chen, J. L. Ma, X. Lu, Z. Jin, R. Kodama, Z. M. Sheng, and J. Zhang, "Bursts of terahertz radiation from large-scale plasmas irradiated by relativistic picosecond laser pulses," *Phys. Rev. Lett.* **114**(25), 255001 (2015).
16. F. Consoli, R. De Angelis, L. Duvillaret, P. L. Andreoli, M. Cipriani, G. Cristofari, G. Di Giorgio, F. Ingenito, and C. Verona, "Time-resolved absolute measurements by electro-optic effect of giant electromagnetic pulses due to laser-plasma interaction in nanosecond regime," *Sci. Rep.* **6**(1), 27889 (2016).
17. A. Poyé, S. Hulin, M. Bailly-Grandvaux, J. L. Dubois, J. Ribolzi, D. Raffestin, M. Bardon, F. Lubrano-Lavaderci, E. D'Humières, J. J. Santos, P. Nicolai, and V. Tikhonchuk, "Physics of giant electromagnetic pulse generation in short-pulse laser experiments," *Phys. Rev. E Stat. Nonlin. Soft Matter Phys.* **91**(4), 043106 (2015).
18. L. Yun-Shik, *Principles of Terahertz Science and Technology* (Springer Science & Business Media, 2009).
19. H. A. Hafez, X. Chai, A. Ibrahim, S. Mondal, D. Férachou, X. Ropagnol, and T. Ozaki, "Intense terahertz radiation and their applications," *J. Opt.* **18**(9), 093004 (2016).
20. R. I. Stantchev, B. Sun, S. M. Hornett, P. A. Hobson, G. M. Gibson, M. J. Padgett, and E. Hendry, "Noninvasive, near-field terahertz imaging of hidden objects using a single-pixel detector," *Sci. Adv.* **2**(6), e1600190 (2016).
21. L. Thrane, R. H. Jacobsen, P. Uhd Jepsen, and S. R. Keiding, "THz reflection spectroscopy of liquid water," *Chem. Phys. Lett.* **240**(4), 330–333 (1995).
22. H. Inouye, K. Tanaka, I. Tanahashi, and K. Hirao, "Ultrafast dynamics of nonequilibrium electrons in a gold nanoparticle system," *Phys. Rev. B* **57**(18), 11334–11340 (1998).
23. P. U. Jepsen, D. G. Cooke, and M. Koch, "Terahertz spectroscopy and imaging - Modern techniques and applications," *Laser Photonics Rev.* **5**(1), 124–166 (2011).
24. B. M. Fischer, M. Walther, and P. U. Jepsen, "Far-infrared vibrational modes of DNA components studied by terahertz time-domain spectroscopy," *Phys. Med. Biol.* **47**(21), 3807–3814 (2002).
25. M. Walther, P. Plochocka, B. Fischer, H. Helm, and P. Uhd Jepsen, "Collective vibrational modes in biological molecules investigated by terahertz time-domain spectroscopy," *Biopolymers* **67**(4-5), 310–313 (2002).
26. L. Razzari, F. H. Su, G. Sharma, F. Blanchard, A. Ayesheshim, H. C. Bandulet, R. Morandotti, J. C. Kieffer, T. Ozaki, M. Reid, and F. A. Hegmann, "Nonlinear ultrafast modulation of the optical absorption of intense few-cycle terahertz pulses in n-doped semiconductors," *Phys. Rev. B* **79**(19), 193204 (2009).
27. H. A. Hafez, I. Al-Naib, M. M. Dignam, Y. Sekine, K. Oguri, F. Blanchard, D. G. Cooke, S. Tanaka, F. Komori, H. Hibino, and T. Ozaki, "Nonlinear terahertz field-induced carrier dynamics in photoexcited epitaxial monolayer graphene," *Phys. Rev. B* **91**(3), 035422 (2015).
28. E. Freysz and J. Degert, "Nonlinear optics: Terahertz Kerr effect," *Nat. Photonics* **4**(3), 131–132 (2010).
29. J. Hebling, K.-L. Yeh, M. C. Hoffmann, and K. A. Nelson, "High-Power THz Generation, THz Nonlinear Optics, and THz Nonlinear Spectroscopy," *IEEE J. Sel. Top. Quantum Electron.* **14**(2), 345–353 (2008).
30. U. Frühling, M. Wieland, M. Gensch, T. Gebert, B. Schütte, M. Krikunova, R. Kalms, F. Budzyn, O. Grimm, J. Rossbach, E. Plönjes, and M. Drescher, "Single-shot terahertz-field-driven X-ray streak camera," *Nat. Photonics* **3**(9), 523–528 (2009).
31. I. Grguraš, A. Maier, C. Behrens, T. Mazza, T. J. Kelly, P. Radcliffe, S. Düsterer, A. K. Kazansky, N. M. Kabachnik, T. Tschentscher, J. T. Costello, M. Meyer, M. C. Hoffmann, H. Schlarb, and A. L. Cavalieri, "Ultrafast X-ray pulse characterization at free-electron lasers," *Nat. Photonics* **6**(12), 852–857 (2012).
32. J. A. Fülöp, L. Pálfalvi, G. Almási, and J. Hebling, "Design of high-energy terahertz sources based on optical rectification," *Opt. Express* **18**(12), 12311–12327 (2010).
33. H. Hirori, A. Doi, F. Blanchard, and K. Tanaka, "Single-cycle terahertz pulses with amplitudes exceeding 1 MV/cm generated by optical rectification in LiNbO₃," *Appl. Phys. Lett.* **98**(9), 091106 (2011).
34. M. Shalaby and C. P. Hauri, "Demonstration of a low-frequency three-dimensional terahertz bullet with extreme brightness," *Nat. Commun.* **6**, 5976 (2015).
35. G. L. Carr, M. C. Martin, W. R. McKinney, K. Jordan, G. R. Neil, and G. P. Williams, "High-power terahertz radiation from relativistic electrons," *Nature* **420**(6912), 153–156 (2002).
36. Z. Wu, A. S. Fisher, J. Goodfellow, M. Fuchs, D. Daranciang, M. Hogan, H. Loos, and A. Lindenberg, "Intense terahertz pulses from SLAC electron beams using coherent transition radiation," *Rev. Sci. Instrum.* **84**(2), 022701 (2013).
37. M. C. Hoffmann and J. A. Fülöp, "Intense ultrashort terahertz pulses: generation and applications," *J. Phys. D Appl. Phys.* **44**(8), 083001 (2011).
38. F. Blanchard, G. Sharma, X. Ropagnol, L. Razzari, R. Morandotti, and T. Ozaki, "Improved terahertz two-color plasma sources pumped by high intensity laser beam," *Opt. Express* **17**(8), 6044–6052 (2009).
39. M. Clerici, M. Peccianti, B. E. Schmidt, L. Caspani, M. Shalaby, M. Giguère, A. Lotti, A. Couairon, F. Légaré, T. Ozaki, D. Faccio, and R. Morandotti, "Wavelength scaling of terahertz generation by gas ionization," *Phys. Rev. Lett.* **110**(25), 253901 (2013).
40. A. V. Balakin, M. S. Dzhdzhoev, V. M. Gordienko, M. N. Esaulkov, I. A. Zhvaniya, K. A. Ivanov, I. A.

- Kotelnikov, N. A. Kuzechkin, I. A. Ozheredov, V. Y. Panchenko, A. B. Savelev, M. B. Smirnov, P. M. Solyankin, and A. P. Shkurinov, "Interaction of high-intensity femtosecond radiation with gas cluster beam: effect of pulse duration on joint terahertz and x-ray emission," *IEEE Trans. Terahertz Sci. Technol.* **7**(1), 70–79 (2017).
41. A. Sell, A. Leitenstorfer, and R. Huber, "Phase-locked generation and field-resolved detection of widely tunable terahertz pulses with amplitudes exceeding 100 MV/cm," *Opt. Lett.* **33**(23), 2767–2769 (2008).
 42. G. Q. Liao, Y. T. Li, Y. H. Zhang, H. Liu, X. L. Ge, S. Yang, W. Q. Wei, X. H. Yuan, Y. Q. Deng, B. J. Zhu, Z. Zhang, W. M. Wang, Z. M. Sheng, L. M. Chen, X. Lu, J. L. Ma, X. Wang, and J. Zhang, "Demonstration of coherent terahertz transition radiation from relativistic laser-solid interactions," *Phys. Rev. Lett.* **116**(20), 205003 (2016).
 43. S. Mondal, Q. Wei, W. J. Ding, H. A. Hafez, M. A. Fareed, A. Laramée, X. Ropagnol, G. Zhang, S. Sun, Z. M. Sheng, J. Zhang, and T. Ozaki, "Aligned copper nanorod arrays for highly efficient generation of intense ultra-broadband THz pulses," *Sci. Rep.* **7**, 40058 (2017).
 44. Z. M. Sheng, K. Mima, J. Zhang, and H. Sanuki, "Emission of electromagnetic pulses from laser wakefields through linear mode conversion," *Phys. Rev. Lett.* **94**(9), 095003 (2005).
 45. Z. Y. Chen and A. Pukhov, "High field terahertz emission from relativistic laser-driven plasma wakefields," *Phys. Plasmas* **22**(10), 103105 (2015).
 46. G. Q. Liao, Y. T. Li, C. Li, S. Mondal, H. A. Hafez, M. A. Fareed, T. Ozaki, W. M. Wang, Z. M. Sheng, and J. Zhang, "Terahertz emission from two-plasmon-decay induced transient currents in laser-solid interactions," *Phys. Plasmas* **23**(1), 013104 (2016).
 47. W. J. Ding and Z. M. Sheng, "Sub GV/cm terahertz radiation from relativistic laser-solid interactions via coherent transition radiation," *Phys. Rev. E Stat. Nonlin. Soft Matter Phys.* **93**(6), 063204 (2016).
 48. A. Gopal, S. Herzer, A. Schmidt, P. Singh, A. Reinhard, W. Ziegler, D. Brömmel, A. Karmakar, P. Gibbon, U. Dillner, T. May, H.-G. Meyer, and G. G. Paulus, "Observation of Gigawatt-Class THz Pulses from a Compact Laser-Driven Particle Accelerator," *Phys. Rev. Lett.* **111**(7), 074802 (2013).
 49. S. R. Ahmed, B. R. Nag, and M. D. Roy, "Hot-electron transport in In_{0.53}Ga_{0.47}As," *Solid-State Electron.* **28**(12), 1193–1197 (1985).
 50. G. Gallot, J. Zhang, R. W. McGowan, T.-I. Jeon, and D. Grischkowsky, "Measurements of the THz absorption and dispersion of ZnTe and their relevance to the electro-optic detection of THz radiation," *Appl. Phys. Lett.* **74**(23), 3450–3452 (1999).
 51. Y. Minami, Y. Hayashi, J. Takeda, and I. Katayama, "Single-shot measurement of a terahertz electric-field waveform using a reflective echelon mirror," *Appl. Phys. Lett.* **103**(5), 051103 (2013).
 52. W. J. Ding, Z. M. Sheng, and W. S. Koh, "High-field half-cycle terahertz radiation from relativistic laser interaction with thin solid targets," *Appl. Phys. Lett.* **103**(20), 204107 (2013).

1. Introduction

High-intensity femtosecond laser-plasma interaction [1,2] is an excellent source of high-energy photons [3,4], electrons [5,6], protons [7] and ions [8]. Development of tabletop sources of such photons and particles are of high interest for the scientific community [5,6,9]. It has also been found that high-intensity femtosecond laser-plasma interaction is a good source of low energy photons, such as intense ultra-broadband THz [10–15] and GHz pulses [16,17]. Generation of broadband intense THz pulses is desirable for various applications [18,19], such as high resolution nearfield THz imaging [20], probing physical, chemical, biological systems [21–25] and revealing nonlinear carrier dynamics in materials [26,27]. High-intensity THz pulses are also opening new areas of science, such as nonlinear optics in the THz regime [19,28,29]. Furthermore, intense THz pulses can be used as the streaking electric field for developing THz-field-driven streak cameras, which can be used to determine the temporal profile of femtosecond X-ray pulses and femtosecond electron bunches [30,31]. Hence, the generation of intense THz pulses has been the object of a great interest since the last decade, and several techniques have been studied in detail [19,32–34]. Highly energetic THz pulses can be generated in electron accelerators, either by bending the accelerated electron beam using external magnetic field [35] or by sending the relativistic energy electrons through a thin titanium foil [36]. However, these facilities are not accessible at moderate laboratory scales at the tabletop level. Among the tabletop THz sources, optical rectification has been the subject of many extensive efforts to scale up both their peak electric field and energy [33,37]. There have also been significant advances in intense THz pulse generation from air plasma [38,39] and by the interaction of high intensity laser with gas cluster [40]. THz pulses with more than 100 MV/cm peak electric field have also been demonstrated by difference-frequency mixing of two parametrically amplified pulses [41].

Another promising method for intense broadband THz pulse generation is high-intensity femtosecond laser-plasma interaction, whose development is starting to emerge [14,42,43]. Using this technique, THz pulse generation with peak electric field of GV/cm has been predicted by particle-in-cell (PIC) simulations [44,45]. Another advantage of such broadband THz pulses is that they are shorter in pulse width and hence possess high peak power and peak electric field. For example, Fourier-transform limited 10 THz bandwidth (FWHM) pulses are 44 fs in width. THz pulses from conventional sources, such as optical rectification and the photoconductive antenna, are often narrowband as well as low frequency, and are several picoseconds in width [19].

In this article, we describe our recent studies on the development and characterization of a tabletop intense broadband THz source based on high-intensity femtosecond laser-plasma interaction on a solid surface at relativistic intensity. With this newly developed THz source, we have demonstrated THz nonlinearity using an open aperture Z-scan experiment by measuring nonlinear THz transmission (THz absorption bleaching) through *n*-doped InGaAs thin film. This technique is then used to estimate the peak THz electric field, which requires the knowledge of the THz pulse profile. To this end, we first numerically simulate a THz pulse based on the THz spectrum measured at the detector position. Then, the THz peak field is estimated through the simulations by reproducing the experimentally observed bleaching in the InGaAs sample. Further measurements of the THz pulse profile have been performed via single-shot detection to further justify our estimate of the THz peak electric field.

2. Experimental setup

A schematic diagram of the experimental setup is shown in Fig. 1. We use the 40 fs, 800 nm, high contrast ratio ($\sim 10^{-7}$, in nanosecond range) Ti:sapphire laser pulse from the 10 TW, 10 Hz beamline of the Advanced Laser Light Source (ALLS). Using an *f*/3 off-axis parabolic mirror, the femtosecond laser is focused onto an unpolished solid copper plate (size: 5 cm \times 5 cm \times 3 mm) to a circular spot of 20 μ m in diameter. The target is mounted on an automated XYZ translation stage inside a vacuum chamber, so that each laser pulse interacts with an intact target surface. The 10 Hz beam line at ALLS can deliver pulse energy up to 240 mJ in 40 fs after compression, and a corresponding peak intensity of about 3.5×10^{18} W cm $^{-2}$ can be achieved at focus. Ultra-broadband THz and infrared (IR) pulses are generated as a result of the laser-plasma interaction [43,46]. The generated THz pulses are then collimated by using a thick gold plated off-axis parabolic mirror, and then guided out of the vacuum chamber through a THz window made of ultrahigh molecular weight polyethylene (UHMWPE) that acts as a low-pass filter with a cut-off at 20 THz. The generated THz pulse is then refocused by another off-axis parabolic mirror on to a pyroelectric detector (Gentec-EO, THZ5I-BL-BNC), to measure the THz pulse energy. In addition to the UHMWPE window, two high-resistivity float-zone silicon (HRFZ-Si) filters have been used to remove any residual visible or near infrared radiation that may have leaked through the UHMWPE window. We take 15 shots average to reduce the statistical error. The THz pulse energy is calibrated, taking into account the transmission of the UHMWPE window and the HRFZ-Si filters used in the experiment. Due to the limited numerical aperture of the off-axis parabolic mirror, the THz pulse energy is collected over a relatively small solid angle of 0.0873 Sr.

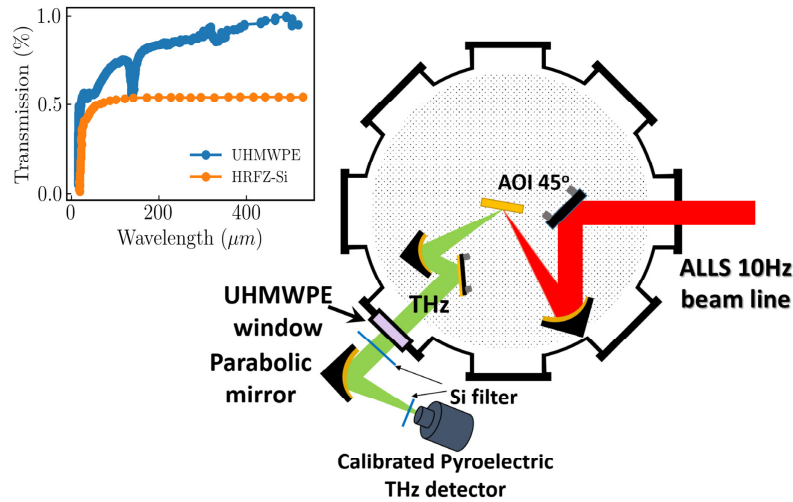


Fig. 1. Schematic of the experimental setup for high electric field THz pulse generation. In the inset THz transmission through HRFZ-Si filter and UHMWPE window is plotted.

3. Results and discussion

We have used five target materials for THz pulse generation: glass, copper, aluminum, graphite and plastic (Perspex). In Fig. 2(a), we show the comparison of THz pulse energy (≤ 20 THz) generated from these targets under the same experimental conditions. We find that glass targets generate relatively weak THz signals (maximum up to $0.5 \mu\text{J}$), whereas strong THz signal is generated from graphite block (maximum up to $6.5 \mu\text{J}$), mainly because of higher coupling of the driving laser energy into the graphite plasma. However, in this article we present data mainly from Cu target.

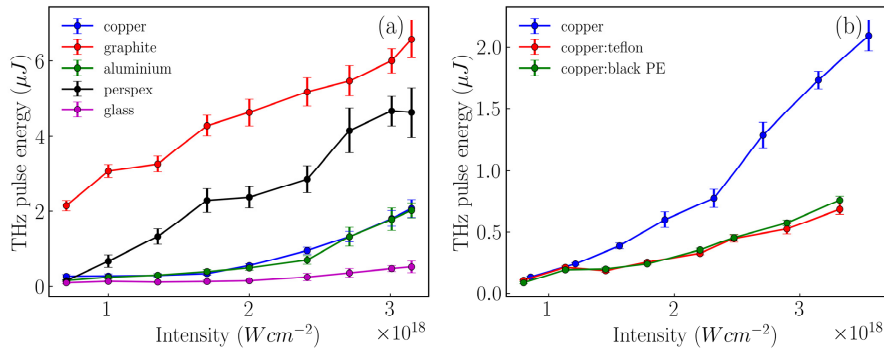


Fig. 2. (a) Comparison of THz pulse energy with laser intensity from various target materials. (b) THz pulse energy generated from unpolished Cu and with low pass filters (≤ 5 THz) at various laser intensity.

In Fig. 2(b), we plot the THz (≤ 20 THz) pulse energy from unpolished Cu target for different laser intensities. We detect a maximum $\sim 2.2 \mu\text{J}$ THz energy in each THz pulse from rough copper targets. Since we collect the signal over a relatively small solid angle of $\Delta\Omega = 0.0873$ Sr and the THz pulses are emitted in a wide angle at the target front [14,43,47], we estimate that more than $100 \mu\text{J}$ pulse energy within the spectral band of ≤ 20 THz has been generated from Cu target. Most of the THz pulse energy can be collected by using an ellipsoidal reflector, as described by Gopal *et al.* [14,48]. In Fig. 2(b), we also show the THz

pulse energy measured at different laser intensities from unpolished Cu target, using black polyethylene and 1 mm thick Teflon filters, which both work as low pass filters. The black polyethylene sheet has cutoff at ~ 5 THz and the 1 mm-thick Teflon filter has cutoff at ~ 6 THz. Although most of the pulse energy remains in the higher frequency range (6 THz – 20 THz), a large part of THz pulse energy ($0.7 \mu\text{J}$) is detected even in the lower frequency range (≤ 6 THz), which is $\sim 30\%$ of the total THz pulse energy generated in the spectral range ≤ 20 THz. The amount of THz pulse energy generated by this technique would be sufficient for many applications. However, a detailed characterization of the THz pulses is required for such application. A full characterization of the THz pulses generated by high-intensity laser-plasma interaction is challenging, due to the low repetition rate and the ultra-broadband spectral span of the THz pulses [19,43].

Electromagnetic pulses generated by high-intensity laser-solid interaction are broadband in nature, with frequencies not only limited in the THz band, but also covering frequencies in to the infrared [14]. In the present setup, we select only the frequency band ≤ 20 THz using the low-pass UHMWPE window (with a low-pass cutoff at 20 THz). We further measure the THz spectrum at the same position of the pyroelectric detector by using a series of narrowband bandpass filters (with bandwidths (FWHM) of 7% to 25% of the central wavelength). The obtained spectrum is shown in the Fig. 3(a). The spectrum was recorded at a laser intensity of $4 \times 10^{17} \text{ W cm}^{-2}$. Each data point in Fig. 3(a) is taken by averaging over 20 laser shots to reduce statistical error. The spectrum captured by such a method shows a peak spectral intensity at 6 THz, with an approximate bandwidth of ~ 7.8 THz FWHM. This is the spectrum of the THz pulse that passes through the UHMWPE window, whereas the generated spectrum can be different, with wider band and different peak spectral intensity [14]. Figure 3(b) (green curve) shows the envelope of the THz pulse in the temporal domain, which has been derived by inverse Fourier transformation of the experimentally recorded THz spectrum shown in Fig. 3(a). A Gaussian fit to the temporal envelope of the pulse results in a temporal width of ~ 60 fs FWHM. Figure 3(b) also shows the mathematically generated THz pulse (orange curve) with a Gaussian envelope (blue curve), which is used in the simulations presented in Sec. 4. All the plots in Fig. 3(b) are normalized to unity for better comparison.

The THz pulses generated in our experiments have a peak at 6 THz as shown in the Fig. 3(a). Hence, a numerically calculated THz focal spot diameter ($2w_0 \approx 213 \mu\text{m}$) corresponding to 6 THz frequency has been used in the numerical simulation.

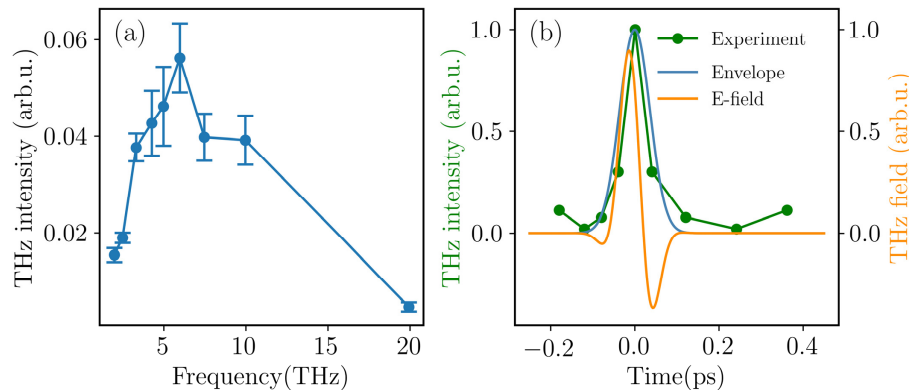


Fig. 3. (a) Experimentally measured power spectrum of the generated THz pulses at the position of pyroelectric detector after filtering with UHMWPE window. The spectrum was measured with a series of bandpass filters. (b) THz pulse (green curve) in the time domain generated by taking the inverse Fourier transform of the spectrum shown in Fig. 3(a), Mathematically generated pulse (orange curve) that is used in the simulations presented in the next section, with a Gaussian envelope (blue curve), which is used in the simulations presented in the next section.

4. Estimation of peak electric field

Estimating the peak THz electric field is crucial for applications of intense THz pulses in research and industry. However, measurement of the peak electric field of the ultra-broadband THz pulses generated by relativistic laser-plasma interaction is challenging. This is because generation of these intense THz pulses often requires high power driving lasers, which are typically limited in repetition rate. Since conventional time-domain electro-optic detection of the THz waveform is achieved by a sequential plot of the signal versus the time delay, it requires long data acquisition, and thus is not suitable for low repetition-rate sources [19]. In addition, THz pulses generated by this technique are ultra-broadband in nature, which indicates that THz pulses are femtosecond in nature and contain high-frequency, and highly intense electric fields. Since the spectral response of many electro-optic crystals is limited, the use of standard electro-optic sampling for electric field measurement of the THz field of ultra-broadband THz sources becomes inefficient.

Here, we present a procedure for estimating the THz peak electric field of intense ultra-broadband THz pulses using nonlinear interactions of THz pulses with a semiconductor. In this section, we demonstrate that THz pulses generated by the above-mentioned technique, with pulse energy $\sim 2.2 \mu\text{J}$, is sufficient to demonstrate THz pulse induced nonlinearity in an n -doped InGaAs thin film. We performed an open aperture Z-scan experiment with the THz pulses generated by this technique with an n -doped InGaAs ($\text{In}_{0.53}\text{Ga}_{0.47}\text{As}$) thin film on a $500 \mu\text{m}$ thick indium phosphate (InP) substrate, in a manner similar to that reported in [26] Razzari et al. The experimental scheme is depicted in Fig. 4(a). The thickness of the InGaAs film is 500 nm and the doping concentration is $2 \times 10^{18} \text{ cm}^{-3}$. We measure the nonlinear change in transmission of the THz pulses while scanning the sample in and out of the focused beam. The experimentally obtained THz transmission curve through InGaAs thin film is shown in Fig. 5(d) (green curve). The THz transmission increases from $\sim 6.5\%$ away from the focus to 11.3% at the focus. We notice that the bare InP substrate has an overall transmission of $\sim 60\%$. Therefore, the THz transmission shown in Fig. 5(d) is plotted after normalization to the InP transmission. Figure 5(e) shows the normalized THz transmission (normalized with THz transmission at 6 mm away from the focus) through the InGaAs thin film, for better comparison with the data from previous experiments by Razzari *et al.* [26].

Next, we demonstrate that one can estimate the peak THz electric field by making use of the nonlinear THz absorption bleaching in n -doped InGaAs, applying the work by Razzari *et al.* [26]. We make use of the nonlinearity in THz transmission due to intervalley scattering of electrons in the conduction band induced by intense THz pulses, to estimate the THz peak electric field. This simple method is advantageous in comparison to standard electro-optic sampling, because it (i) requires only a few THz pulses for measurement, and thus is suited for low repetition-rate sources, (ii) is not limited by the spectral bandwidth of the THz pulse, and (iii) the THz transmission can easily be measured using pyroelectric detectors. The only disadvantage of this method is that we can only evaluate the peak THz electric field, whereas electro-optic sampling can reveal the complete temporal profile of the THz electric field.

The increase in THz transmission in Figs. 5(d) and 5(e) is due to the THz-electric-field-induced scattering of carriers from the Γ valley to the satellite X valley and L valley of the conduction band, as explained in Fig. 4(b). Carriers in the upper (X and L) valleys have significantly higher effective masses (the effective masses in the Γ and L valleys are $m_{\Gamma 0}^* = 0.03745m_e$ and $m_{L 0}^* = 0.26m_e$, respectively [49]). Therefore, scattering of carriers from the Γ to the L valley due to the intense THz field results in the reduction of the photoconductivity of the sample, thus increasing the transmission of the THz field (THz absorption bleaching).

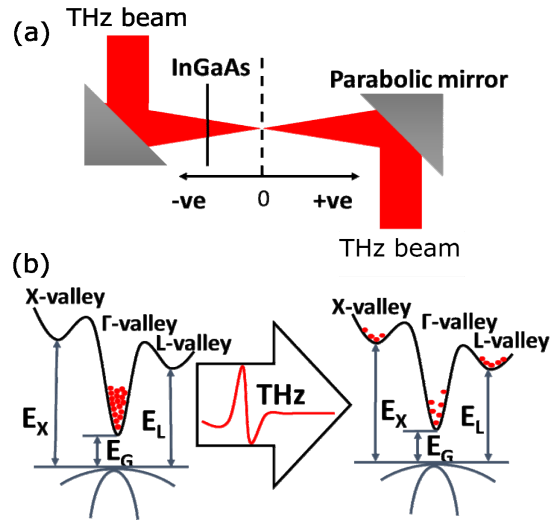


Fig. 4. (a) Schematic diagram of open aperture nonlinear THz transmission measurement. InGaAs thin film on InP substrate is scanned in and out through the focus and THz transmission is measured (b) Schematic diagram to describe nonlinear absorption bleaching. Conduction band of the InGaAs contains several satellite valleys, Γ , X & L valley. Carriers in Γ -valley inside the conduction band bleached to X-valley and L-valley when an InGaAs thin film is exposed to intense THz pulse.

We performed simulations to estimate the peak THz field based on a simple Drude model [26]. A transform limited THz pulse has been modeled mathematically (Fig. 3(b), blue and orange curves) with spectrum and bandwidth similar to those used in the experiment (as shown in Fig. 3(a)). This pulse has been used to simulate the THz transmission through the $\text{In}_{0.53}\text{Ga}_{0.47}\text{As}$ thin film, and the peak electric field associated with the THz pulse is varied until the simulated THz transmission matches with the measurement. Figure 5 summarizes the simulation results. Figure 5(a) shows the variation of the numerically calculated absolute THz transmission (%) through the InGaAs thin film as a function of the peak field and carrier envelope phase ($\text{CEP} = \phi_{\text{CEP}}$) of the THz pulses. The CEP determines the shape of THz field inside the pulse envelope. The color axis represents THz transmission (%) through the InGaAs thin film. The THz transmission strongly depends on the peak electric field as well as the CEP of the THz pulse. For a definite CEP, the absolute THz transmission gradually increases with the peak THz field followed by a saturation in the THz transmission. For a specific peak field, maximum THz transmission is observed at $\phi_{\text{CEP}} = 0$ phase, which indicates that $\phi_{\text{CEP}} = 0$ is highly efficient for intervalley scattering.

Figure 5(b) shows the normalized THz transmission through the InGaAs thin film as a function of the THz peak field and the CEP (ϕ_{CEP}) of the THz pulses. In this case, the THz transmission is normalized to the absolute THz transmission at 6 mm away from the focus. For higher THz fields (> 0.88 MV/cm), the normalized THz transmission is no longer maximum at $\phi_{\text{CEP}} = 0$. This behavior of the normalized THz transmission can be explained by the partial saturation in the intervalley scattering at focus. At higher peak electric fields, the rate at which the absolute THz transmission increases with peak field slows down due to partial saturation in intervalley scattering. However, the electric field is substantially lower at 6 mm away from the focus where the normalization transmission is measured, due to larger spot size and in turn less THz field-induced intervalley scattering. Hence, while increasing peak THz field, the normalized THz transmission through InGaAs thin film falls down at large THz peak field and for smaller ϕ_{CEP} .

By measuring the THz transmission through the InGaAs thin film and using reverse calculation, we can also estimate the THz peak field. However, estimating the peak electric field of the THz pulse depends on the CEP (ϕ_{CEP}) of the optical cycle in the pulse envelope,

due to the CEP dependence of THz transmission through InGaAs thin film (Figs. 5(a) and 5(b)). This behavior affects the estimation of the THz electric field through nonlinear THz transmission (THz absorption bleaching) measurements, as shown in Fig. 5(c). We show in Fig. 5(c) the evaluated THz fields at focus as a function of the THz CEP (ϕ_{CEP}) for two different cases, with spectral ranges ≤ 20 THz and ≤ 3 THz. For the first case, which is marked by the spectral range ≤ 20 THz, we choose a THz pulse similar to the one shown in Fig. 3(b), and vary its CEP. For the latter, the THz pulse has a similar spectrum but with a cutoff at 3 THz. The additional ≤ 3 THz spectral range is chosen to compare the data from single-shot measurement described in section 5, which has spectral sensitivity up to 3 THz. These simulations are performed with a cosine CEP varied from $-\pi$ to π . Using this simple method, the peak electric field can be estimated, and we evaluate a THz peak electric field at focus to be at least 0.5 MV/cm for the spectrum (≤ 20 THz) recorded in Fig. 3(a) and THz pulse in Fig. 3(b). The peak electric field at focus is minimum (0.5 MV/cm) for $\phi_{\text{CEP}} = 0$, and maximum (3.76 MV/cm) for $\phi_{\text{CEP}} = \pm 0.66\pi$ for the same spectral band. For the spectral range ≤ 3 THz, the maximum and minimum THz field at focus is found to be 3.78 MV/cm and 20kV/cm for $\phi_{\text{CEP}} = \pm 0.55\pi$ and $\phi_{\text{CEP}} = 0$, respectively. The large difference between the evaluated THz peak fields at $\phi_{\text{CEP}} = 0$ and $\phi_{\text{CEP}} \sim 0.5\pi$ is directly correlated to the intervalley scattering of carriers in InGaAs thin film by the THz pulse. The THz field inside a Gaussian envelope that is used in the simulation consists of a large peak for $\phi_{\text{CEP}} = 0$ while using a cosine carrier envelope phase. Due to its one large peak, this type of THz pulse is favorable for massive intervalley scattering and as a result a lower THz peak field is capable to induce large amount of THz transmission. This behavior is also reflected in the THz transmission shown in Fig. 5(a). Hence, while we reverse calculation for THz peak field associated with the pulse using experimentally measured THz transmission, we obtain the lowest THz peak field for the case $\phi_{\text{CEP}} = 0$. In a similar manner, the THz pulse with $\phi_{\text{CEP}} \sim 0.5\pi$ phase is composed of two peaks, one positive and one negative peak of same amplitude inside the pulse envelope providing net field is zero. Hence, net intervalley scattering is significantly less in this case and such THz pulses are not suitable for nonlinear absorption bleaching in InGaAs thin film. As a result, while we calculate for THz peak field associated with the THz pulse using experimentally measured THz transmission we get large THz peak field.

Figures 5(a) and 5(c) show that the estimation of the THz peak field strongly depends on the CEP (ϕ_{CEP}) of the THz electric field. To resolve this uncertainty, a single-shot measurement technique to capture the temporal profile of the THz pulse is developed and described in detail in section 5. We plot in Fig. 5(d) the experimentally obtained and numerically calculated THz transmission through InGaAs thin film, while the sample is scanned through the focus. All the experimentally captured THz pulse profiles in single-shot THz detection are tested in our simulations to reproduce the THz transmission through InGaAs. The best fit is shown in Fig. 5(d), and is obtained by employing the data of Shot 7 in Table 1. The corresponding THz peak electric field is estimated to be 2.5 MV/cm. In Fig. 5(e) we show the experimentally obtained and numerically calculated normalized THz transmission through InGaAs thin film while the thin film is scanned through the focus.

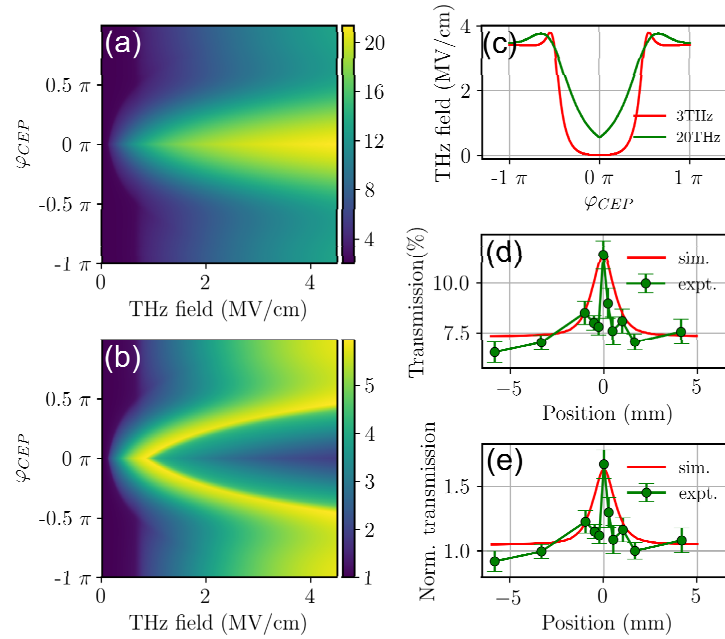


Fig. 5. (a) Absolute transmission of THz pulses through InGaAs thin film for a numerically generated THz pulse shown in Fig. 3. The color axis corresponds to percentage of transmission. (b) Normalized THz transmission (normalized to THz transmission at -6 mm) through InGaAs thin film as a function of different peak field and carrier envelope phase (ϕ_{CEP}). (c) THz peak electric field at focus as a function of CEP of THz pulses for two different spectral ranges ≤ 3 THz and ≤ 20 THz. The THz field is calculated using the experimentally recorded THz transmission at focus shown in Fig. 5 (d). Experimentally (green) and numerically (red) obtained (d) absolute THz transmission and (e) normalized THz transmission through InGaAs thin film while the sample is scanned through focus.

5. Verification of THz peak field with experimentally obtained THz pulse profile

Experimental measurement of the temporal profile of the THz pulses is challenging for relativistic laser-plasma sources, because of the following reasons:

1. THz pulses generated by this method are broad-band in nature. For example, the spectrum of the pulses at the detector position is shown in Fig. 3(a) and has a bandwidth of 7.8 THz FWHM with a peak around 6 THz. With this bandwidth, the transform limited THz pulses are expected to be sub-picosecond in duration.
2. Relativistic intensity laser-plasma interactions require high-power lasers, which are also generally of low repetition rate and have lower shot-to-shot stability compared to kHz class lasers. In many cases, these experiments are performed in single-shot mode. Hence, THz pulses generated here are also of low repetition rate and less stable, and hence are not suitable for most of the THz detection techniques that were initially developed with highly stable kHz laser systems.

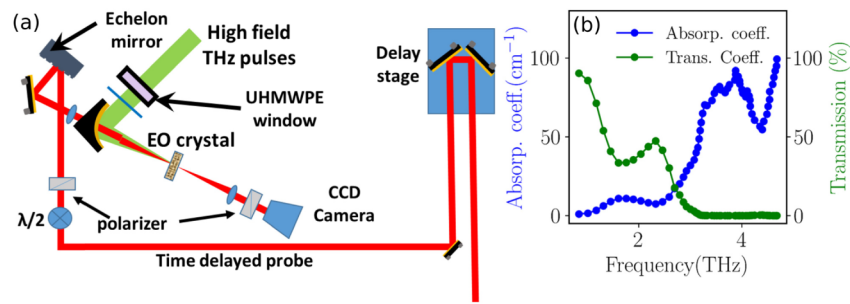


Fig. 6. (a) Single-shot THz measurement setup developed at INRS-ALLS. The THz measurement technique is based on electro-optic sampling using a 1 mm thick zinc telluride (ZnTe) crystal. The temporal delay has been incorporated by using reflective echelon mirror and a CCD camera has been used as a space resolved detector. (b) THz transmission through 1 mm thick ZnTe, which is calculated using data from [50], Gallot, *et al.*

For these reasons, single-shot electro-optic sampling of the THz pulse profile is performed using a technique described by Y. Minami *et al.* [51]. The complete schematics of this experiment is shown in Fig. 6(a). Intense THz pulses generated by high-intensity laser-plasma interaction is collimated out of the chamber through a UHMWPE window, which has a sharp cutoff at 20 THz. The THz pulse is then refocused on a 1 mm thick EO crystal (Zinc Telluride (ZnTe)) by another off-axis mirror. The spectral response of the detection system is determined by the spectral response of the electro-optic crystal. In the present case, the spectral response is limited to be below 3 THz, i.e. much lower than the cutoff (20 THz) of our newly developed THz source. Figure 6(b) shows the calculated transmission of the THz pulses through 1 mm thick ZnTe crystal, using experimentally measured THz absorption coefficients [50].

A part of the main beam, extracted by a 1% beam splitter after compression, is collimated and used as a probe for electro-optic sampling. The polarization contrast of the probe is improved by using a thin polarizer. A reflective echelon mirror, with dimension: step height (H) of $5\mu\text{m}$, step width (W) of $20\mu\text{m}$ and total number of 500 steps, splits the probe beam into 500 beamlets in space, with a delay between two adjacent beamlets of 17 fs. Hence, the horizontal cross-section of the probe beam is converted to temporal delay and enables single-shot electro-optic detection of the THz pulses. The beamlets are focused onto the electro-optic crystal through a small hole in the off-axis mirror. A spatial overlap between the THz and the probe beam is maintained throughout the experiment. A Glan-Taylor calcite polarizer is used to capture changes in the polarization due to electro-optic effect within the ZnTe crystal. A calibrated CCD camera has been used as the 2D detector.

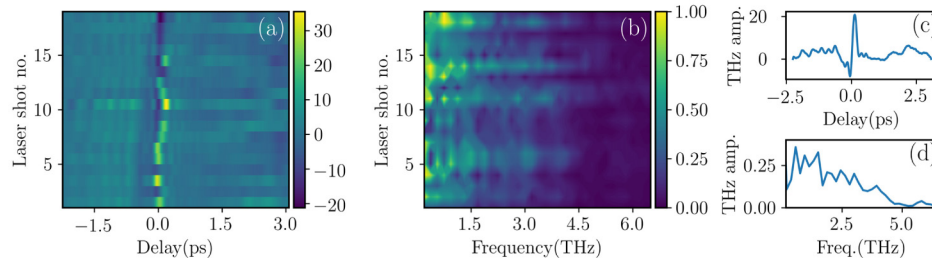


Fig. 7. THz pulses in (a) temporal domain and (b) in frequency domain measured in single-shot THz measurement for 20 successive laser shots. THz pulse profile (c) temporal domain & (d) frequency domain for shot no. 7.

Figure 7(a) shows the temporal profile of the THz pulses for 20 successive laser shots. The color axis represents the THz intensity in arbitrary units. Large pulse-to-pulse

fluctuations have been observed. The carrier envelope phase (ϕ_{CEP}) between any two THz pulses varies significantly from shot to shot, as shown in Fig. 7(a). The CEP (ϕ_{CEP}) for each THz pulse has been estimated by the cosine fit with a Gaussian envelope to a locally selected region near the peak of the pulse profile and is shown in Table 1. Due to complicated THz pulse structure in shots no. 4 and 15, it was not possible to find any cosine function fit to estimate the CEP (ϕ_{CEP}) and we leave the table entry blank. The pulse width of the THz pulses varies between 450 fs and 780 fs as well (width of the largest peak varies between 130 fs and 390 fs), which is found to be very close to the simulation result reported by Ding *et al.* [52]. Slight disagreement is found due to the spectral limitation of the ZnTe crystal (≤ 3 THz). Due to the lower spectral sensitivity (≤ 3 THz) of the detection system, these measured THz pulse profiles are longer than the actual pulse duration. However, we expect that the carrier envelope phase (ϕ_{CEP}) of the THz pulses with 20 THz cutoff will not differ much with the measured ones. Therefore, these THz pulse profiles can be used in the simulation to calculate THz peak field for the THz pulses with the bandwidth shown in Fig. 3(a) without a significant error. Figure 7(b) shows THz pulses in the frequency domain, which is found to be less than 4 THz. These measured THz pulse profiles are then used for THz peak field estimation and is listed below in Table 1. Experimentally generated THz pulses sometimes are not exact sinusoidal and hence in some laser shots the estimated peak THz field exceeds 3.78 MV/cm which is the maximum THz peak field calculated with cosine THz field.

Table 1. THz peak field estimated by using experimentally obtained THz pulse profile in a single-shot electro-optic THz detection.

Shot no.	Shot 1	Shot 2	Shot 3	Shot 4	Shot 5	Shot 6	Shot 7	Shot 8	Shot 9	Shot 10
THz peak field (MV/cm)	0.4	4.9	0.4	4.9	0.8	0.2	2.5	1.8	5.7	1.5
Estimated ϕ_{CEP}	0	$-\frac{\pi}{2}$	0		$-\frac{\pi}{6}$	$-\frac{\pi}{12}$	$-\frac{\pi}{6}$	$-\frac{\pi}{4}$	$-\frac{3\pi}{4}$	$-\frac{\pi}{6}$
Shot no.	Shot 11	Shot 12	Shot 13	Shot 14	Shot 15	Shot 16	Shot 17	Shot 18	Shot 19	Shot 20
THz peak field (MV/cm)	1.4	1.1	4.4	0.01	3.2	5.5	6.3	2.4	3.9	6
Estimated ϕ_{CEP}	$-\frac{\pi}{4}$	$-\frac{\pi}{12}$	$+\frac{11\pi}{12}$	$-\frac{\pi}{3}$		$-\pi$	$-\pi$	$+\frac{11\pi}{12}$	$+\frac{11\pi}{12}$	$+\frac{3\pi}{4}$

THz pulse profile corresponding to shot no. 7 is shown in Figs. 7(c) and 7(d). Good agreement between the experimentally obtained and numerically calculated THz transmission in Fig. 5(d) indicates that a large number of THz pulses are generated with pulse profile close to the one shown in Fig. 7(c) and 7(d).

6. Summary

In summary, we have developed an intense broadband THz source based on high-intensity femtosecond laser-plasma interaction at relativistic intensity. THz pulses generated by this interaction are ultra-broadband in nature, but in this experiment, only ≤ 20 THz spectral band has been chosen by using UHMWPE window. At the detector position, the THz pulses have a bandwidth of 7.8 THz FWHM with a peak around 6 THz. With this bandwidth, these THz pulses are subpicosecond in nature, which increases the peak intensity of the THz pulses generated by this technique. We have also demonstrated that ~ 2.2 μJ of THz energy, collected within a relatively small solid angle of 0.0873 Sr, is sufficient to introduce nonlinearity in

THz transmission through n -doped InGaAs thin film. Further, we have shown that nonlinear THz absorption bleaching in InGaAs can be used to estimate the peak electric field of the THz pulses, which is evaluated to be at least 0.5 MV/cm. This peak field estimation is strongly dependent on the carrier envelope phase (ϕ_{CEP}) of the THz pulse. A single-shot THz pulse detection is developed and the experimentally measured THz field profile have been used for peak electric field estimation for 20 successive laser shots. Experimentally recorded THz pulse profile has also been successfully used to numerically reproduce the experimentally observed absorption bleaching in the InGaAs film through an open aperture Z-scan experiment, which is performed to demonstrate THz nonlinearity.

Funding

Fonds de recherche du Québec – Nature et technologies (FRQNT); Natural Sciences and Engineering Research Council of Canada (NSERC).

Acknowledgment

The authors acknowledge Prof. Ikufumi Katayama for his suggestion in the development of single-shot electro-optic THz detection setup.